Iraqi Geological Journal *Thamsi et al.* *2025, 58 (1D), 1-17*

Iraqi Geological Journal

Journal homepage: https://www.igj-iraq.org

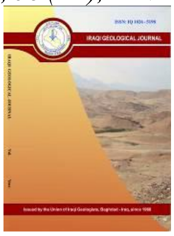

Geochemistry of Iron Ore in Kadong-Kadong, South Sulawesi, Indonesia

Alam B. Thamsi[1*], Muhamad H. Wakila[1], Lamatinulu Ahmad[2] and Muhammad Aswadi[3]

[1] Department of Mining Engineering, University of Muslim Indonesia, Makassar, Indonesia
[2] Department of Industrial Engineering, University of Muslim Indonesia, Makassar, Indonesia
[3] Department of Geological Engineering, Tadulako University, Palu, Indonesia
[*] **Correspondence:** alambudiman.thamsi@umi.ac.id

Received: 4 September 2024
Accepted: 2 March 2025
Published: 30 April 2025

Abstract

Iron (Fe) is an element present in every rock; its availability in large quantities and economic value involves geological processes related to mineralization zoning. Economical iron ore is generally in the form of magnetite (Fe3O4), hematite (Fe2O3), limonite (Fe2O3.H2O), and siderite (FeCO3). Iron ore deposits can be formed primary or secondary. The formation of primary iron ore can occur through magmatic, contact metasomatic, and hydrothermal processes; secondary iron ore deposits are formed by sedimentary, residual, and oxidation processes. This research aims to determine the content of major elements, trace elements, rare earth elements, rock types, magma series, and geotectonic environment in iron ore deposits in the Kadong-kadong Area, Luwu Regency, South Sulawesi Province, based on geochemical data. The research method was carried out in the field. Laboratory analysis uses ICP MS/OES analysis. The results show the highest major oxide composition is the SiO2 compound, which is 54.81%. The second highest major oxide composition is the Al2O3 compound, which is 17.81%. The highest major element composition is Fe, which is >50%. The second highest major element composition is Al at 92,700 ppm. The highest tracer element composition is Ti element, which is 3280 ppm. The second tracer element composition is Mn 1170 ppm. Some elements, such as Ba, U, and Pb, show very significant enrichment. The data show that the study area is rich in rare earth elements, especially in heavy rare earth elements such as Dy, Ho, and Er. The results also show that the chemical composition of the research area shows that the rock types are andesite and basaltic andesite based on the TAS diagram. The SiO2-K2O and Co-Th diagrams show that the rock properties belong to the tholeiite series rock types. The Ta/Yb-Th/Yb diagram shows that the tectonic environment is in a volcanic arc with a tholeiitic magma series.

Keywords: Iron ore; Geotectonic; Magma Series; GCDkit; Kadong-kadong

1. Introduction

Iron ore is one of the most important mineral resources, especially as the steel industry's main raw material supporting various development sectors (Rochani et al., 2008; Shah et al., 2021). Significant iron ore potential exists in Indonesia, especially in the Kadong-kadong area, Luwu Regency, South Sulawesi Province (Thamsi et al., 2021). However, to make the most of this potential, an in-depth understanding of the chemical characteristics of iron ore is required, including the analysis of Major Elements, Tracer Elements, and Rare Earth Elements (REE) (Tamehe, 2019; Zarasvandi et al., 2016). This understanding is important for determining the quality of iron ore, its economic potential, and the geological influences that may have contributed to its formation (Duan, 2014; Hou, 2014; Osterholt, 2018).

Research on iron ore's chemical characteristics has been widely carried out in various regions of Indonesia (Abbas, 2022, 2021; Bakri, 2023; Chaerun, 2017; Soedarsono, 2013). Previous studies have generally focused on the analysis of key elements such as iron (Fe), silica (Si), aluminium (Al), and magnesium (Mg) that play a role in determining the quality of iron ore (Poojari et al., 2023; Spier et al., 2007). In addition, some studies have also examined trace elements that can provide clues about geological processes, such as sedimentation and hydrothermal activity (Chaerun, 2015; Gao, 2017; Kusnadi, 2018). Research on Rare Earth Elements (REEs) in iron ore has also been conducted, especially given its high economic value and application in advanced technology (Aliyari, 2020; Atapour, 2020; Han, 2012). However, most of this research focuses on certain areas and does not specifically cover the Kadong-kadong area.

The research gap is that there is no comprehensive study that simultaneously examines major elements, trace elements, and REEs in iron ore from the Kadong-kadong area. Previous studies have generally only focused on one of these aspects or different regions (Thamsi et al., 2021). The novelty of this study lies in the geochemical analysis method, which provides a complete picture of the characteristics of iron ore in the region. Thus, this research will provide a scientific contribution to understanding iron ore geochemistry and mineralogy and open up new opportunities for exploring and developing a more value-added mining industry in Luwu Regency and its surroundings. The results of this study are expected to serve as a reference for developing a more efficient and effective iron ore exploitation strategy and encourage innovation in mineral utilization in Indonesia.

2. Sample and Analytical Methods

The research location is in Kadong-kadong Sub-district, Luwu Regency, South Sulawesi Province. The research methodology is field sampling and laboratory analysis, by combining the results of literature review, field data, and computational laboratory research results that are comprehensively reviewed, analyzed, and synthesized to formulate a conclusion about the characteristics of the main elements, tracers, and rare earths in iron ore deposits. Sampling in the field was carried out by taking ore data and rock outcrops. The data taken are iron ore data, sampling, rock description in the field and documentation. Sampling in the field is in the form of hand specimens (Hakim et al., 2024; Wakila et al., 2024). The sampling pattern is taken randomly stratified. Samples that have been obtained in the field are then prepared to be sent to the laboratory (Dong, 2021; Wang, 2022).

Data analysis activities are divided into two types of activities: XRF (X-ray Fluorescence) and ICP-OES/MS (Inductively Coupled Plasma - Optical Emission Spectrometry/mass spectrometry) (Gerlitzki, 2023; Han, 2012; Wang, 2024). The purpose of this analysis is geochemical characterization, namely by knowing the main oxides, main elements and trace elements of iron ore in the research area (Keshava et al., 2020; Li, 2014). The location of the sample analysis was at the Laboratory of PT Intertek Utama Sevices Jakarta, Indonesia. Analytical data from the laboratory was then processed using GCDkit software to interpret the data in accordance with the research objectives (Dwivedy, 2021; Karimi, 2021).

3. Results

3.1. Regional Geology

The research area is located in the middle of the southern arm of Sulawesi Island and is regionally part of the eastern side of Sundaland, which borders the Australian plate. The confluence between these two plates affects the geology of the area, including tectonic conditions, geological structure, basin formation, as well as various types of rocks (Hall, 2013). Fig. 1 illustrates the sequence of rocks at the research site that date from the Mesozoic to the Quaternary (Coffield et al., 1993; Djuri et al., 1998). The oldest rocks are composed of rocks that undergo mild to moderate metamorphism, such as schist, gneiss, filet, and shale. These rocks are overlaid by pyrite, quartzite, metamorphic claystone, and alabaster from the Cretaceous Latimojong Formation (Coffield et al., 1993; Djuri et al., 1998; White et al., 2017). Above it is the Toraja Formation, which is deposited in the inner neritic environment and is informally divided into two parts. The bottom is composed of grey to reddish-brown shale, claystone, and limestone, as well as some quartz, conglomerate, and coal sandstone.

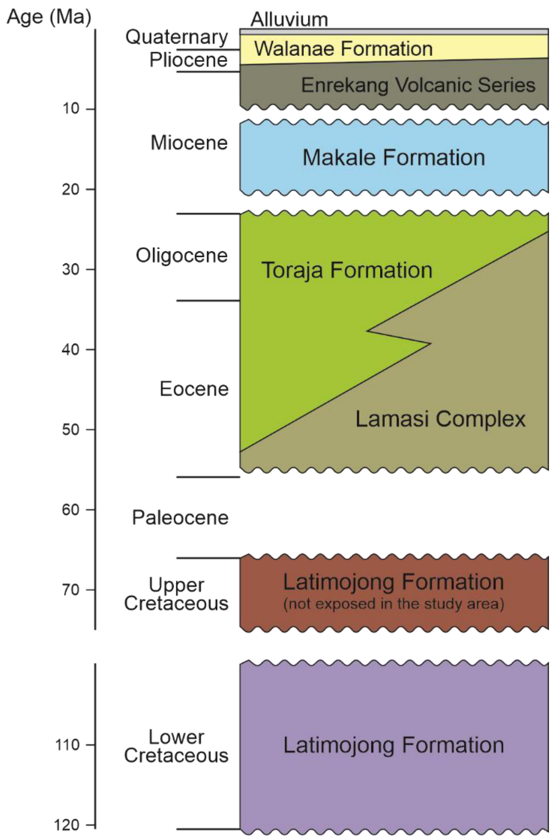

Fig. 1. General stratigraphic column of the Enrekang area and its surroundings (Djuri et al., 1998; White et al., 2017)

The upper layer of the Toraja Formation contains white to grey limestone (Coffield et al., 1993; Djuri et al., 1998; White et al., 2017) with the age of the Eocene to the Oligocene (White et al., 2017). During the Early to Middle Miocene, there was an accumulation of limestone layers of reef and napal in the Makale Formation (White et al., 2017). The Buakayu Formation marks the transition phase from carbonate sedimentation in the upper part of the Makale Formation to a period of volcanism (White et al., 2017).

Volcanic activity during the Miocene to Pliocene produced the Enrekang Vulcanic Series, which covers most of central West Sulawesi (Coffield et al., 1993; Djuri et al., 1998). After that, the Walanae Formation was formed, dominated by carbonate sediments such as limestone and calcareous clay (Coffield et al., 1993). The youngest rock unit in the area is the Quaternary Rock (Djuri et al., 1998). The distribution of rocks in the study area has been remapped by White et al. (2017) (Fig. 2).

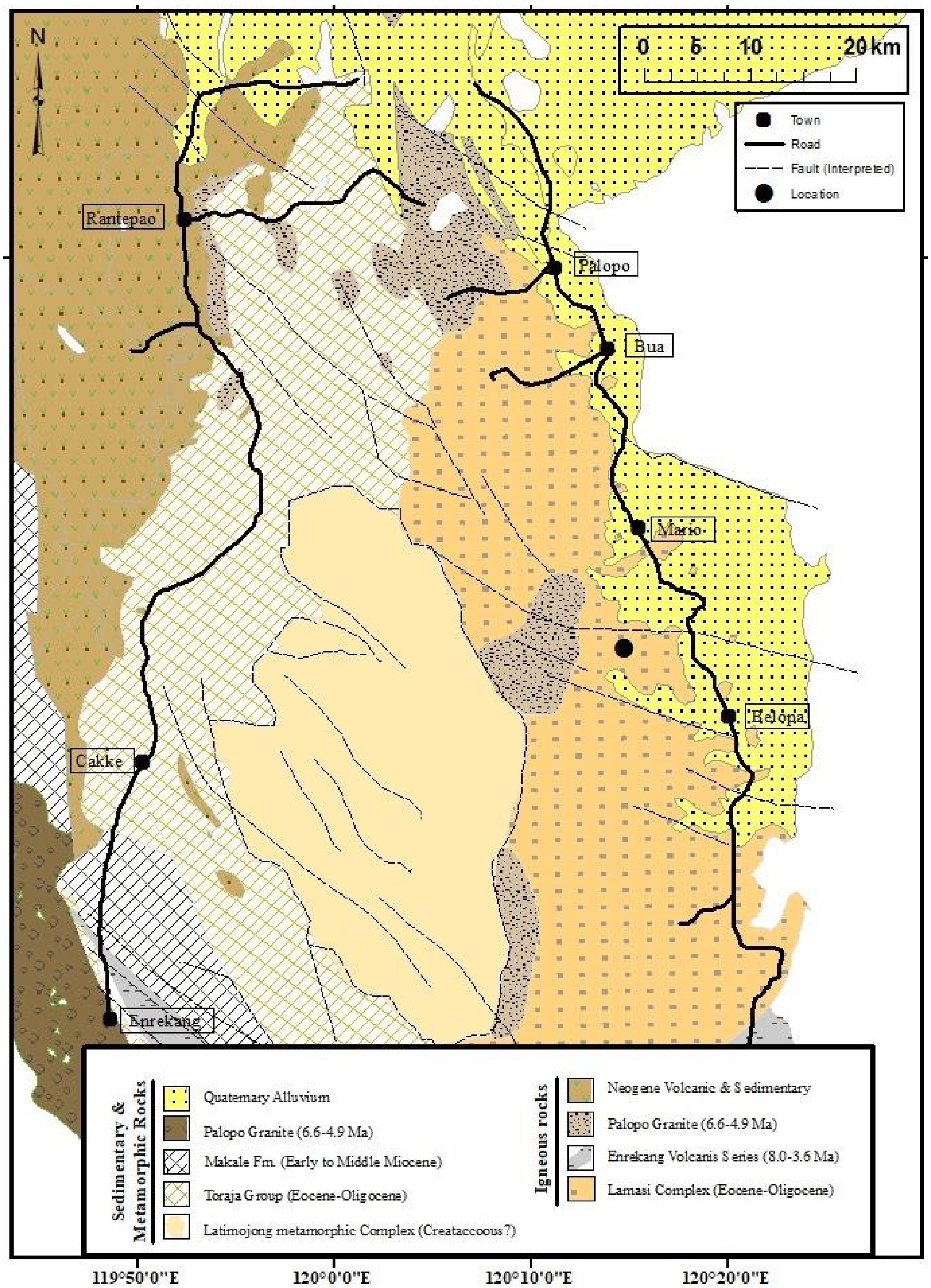

Fig. 2. Regional geological map of the study area (Djuri et al., 1998; White et al., 2017)

3.2. Field Conditions in the Research Area

The research area has a hilly topography with plains that vary from sloping to slightly steep. In this area, a large Bajo River flows along the West Bajo District, Luwu Regency. Most of the land in the study area is used by the community for plantations and rice fields (Fig.3). However, some areas are still in the form of natural forests that humans have not touched. The location of rock sampling is in the Kadong-kadong area. The sampling location can be seen in Fig. 3.

3.3. Geochemistry of Research Area

Fig. 3. Field conditions of the research area

Geochemical data from the research sample are available in Table 1. This data describes the geochemical characteristics of the rocks in the study area. Based on the total alkaline silica (TAS) classification according to Cox et al. (1979), the study area has rocks classified as basaltic andesite rocks (Fig.4) (Philpotts and Ague, 2022).

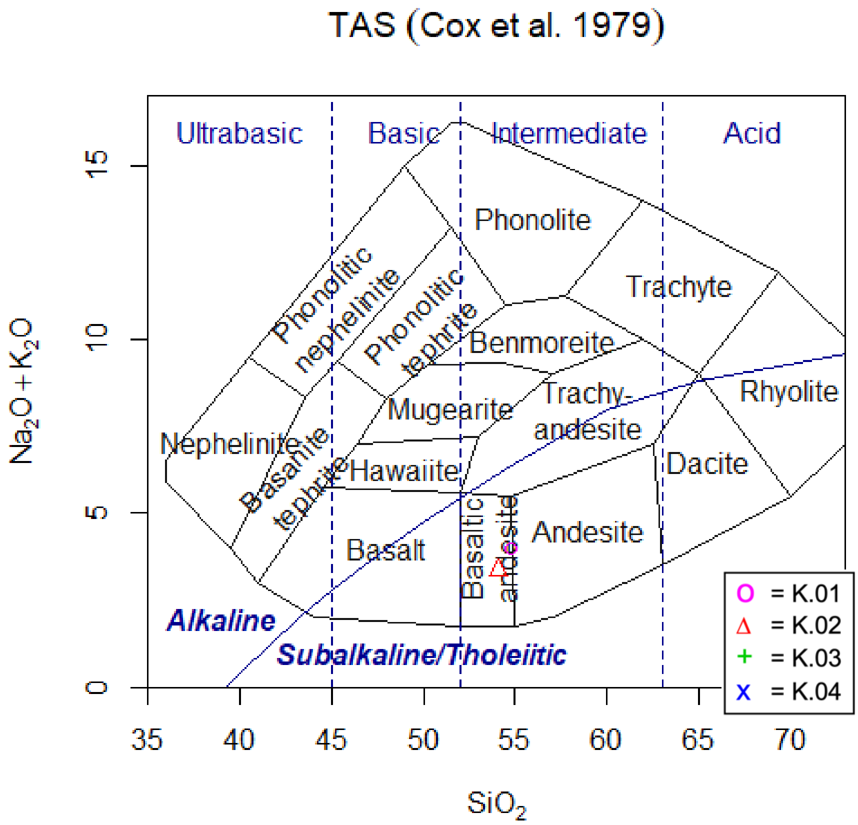

Fig. 4. TAS classification for volcanic rocks modified from Cox et al., 1979

This classification uses Na2O + K2O data as the X-axis and SiO2 as the Y-axis. Major oxide data shows that the content of Na2O compounds is 3.84% - 68.63%, the content of K2O compounds is 0.02% - 0.15%, and the content of SiO2 compounds is 54.10% - 68.63% (Cox et al., 1979; Hanžl et al., 2023).

The Jansen classification 1976 showed that the rocks in the study area were basalt and andesite (Fig. 5). This classification uses geochemical data of Fe+Ti, Al, and Mg elements (Jensen, 1976). Data on the chemical content of Fe elements 3.65% to >50% or equivalent to 36,500 ppm to >500,000 ppm. Ti has a content of 210 ppm to 3280 ppm. The element Al has a content of 9,710 ppm to 9,270 ppm. The content of Mg is 3,160 ppm to 35,700 ppm (Godang et al., 2021).

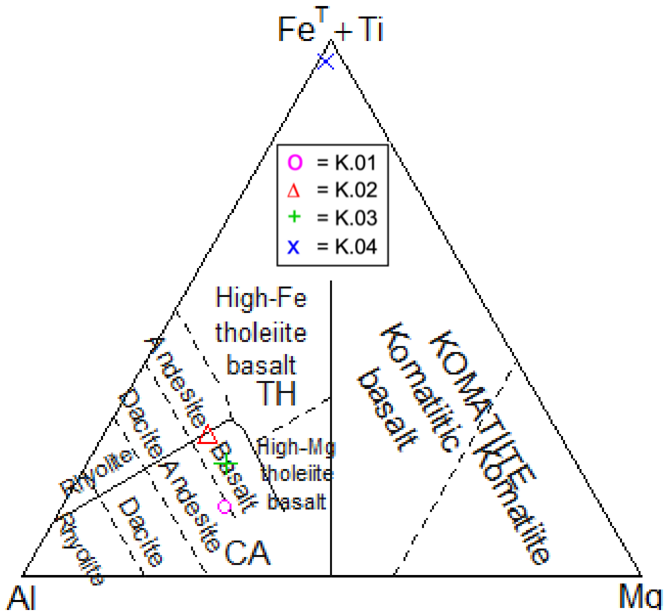

Fig. 5. Classification of rocks (Fe+Ti, Al, and Mg) modified from Jansen (1976)

3.4. Major Element and Major Oxide Variations

Table 1 shows data that the content of SiO2 compounds is 7.28% to 54.81%. The highest content of SiO2 compounds was in the K.01 sample. The variation in SiO_2 content (7.28% to 54.81%) suggests differences in the mineral composition and lithology of the samples. The high SiO_2 content in the K.01 sample indicates the presence of silica-rich minerals, such as quartz or silicate minerals like feldspar or mica. This is often associated with felsic or intermediate igneous rocks (Winter, 2014). The second highest content is occupied by the content of Al2O3 compounds, which is 1.67% to 17.81%. The highest Al2O3 content was in the K.01 sample (Fig. 6). The Al_2O_3 content (1.67% to 17.81%) reflects the presence of aluminium-bearing minerals such as feldspar, clay minerals, or aluminosilicates. The highest Al_2O_3 content in the K.01 sample suggests a greater concentration of such minerals. The highest elemental content is Fe, with 40,100 ppm to >500,000 ppm or 4.01% to >50%. The highest Fe content was in the K.04 sample. This suggests the presence of iron-rich minerals such as hematite, magnetite, or iron sulfides. The second highest chemical content is Al, with 9,710 ppm to 92,700 ppm. The highest Al content was in the K.01 sample (Fig. 6).

In the research area, the properties of the rocks are included in the type of tholeiite series rocks shown in the diagram of SiO2-K2O Peccerillo and Taylor in 1976 (Fig. 7) (Peccerillo and Taylor, 1976). The Tholeiitic series is one of the two main series in the classification of basaltic magma, which is distinguished by its mineralogical and chemical composition (Carlson et al., 2018; Vermeesch and Pease, 2021). The tholeiitic series is rich in iron and a small amount of alkaline elements (such as sodium and potassium) (Gest and McBirney, 1979; Ghoneim, 2023). One of the most prominent characteristics

Table 1. Geochemistry of the research area (ICP-MS/OES and XRF)

Geochemistry		K.01	K.02	K.03	K.04	Geochemistry		K.01	K.02	K.03	K.04
Al	ppm	92700	89300	56800	9710	Ce	ppm	2.1	1.3	2.1	0.3
Ca	ppm	60000	25500	20200	8110	La	ppm	0.6	0.4	0.8	<0.1
Na	ppm	28700	25200	11600	540	Nd	ppm	2.5	1.8	2.7	0.3
Fe	ppm	36500	80100	40100	>500000	Pr	ppm	0.41	0.26	0.41	<0.05
K	ppm	1170	1080	110	40	Sm	ppm	1.1	0.9	1.3	0.1
Mg	ppm	35700	23900	20500	3160	Eu	ppm	0.5	0.3	0.4	<0.1
Total Major Element	ppm	254770	245080	149310	521560	Gd	ppm	1.9	1.7	2.3	0.2
Mn	ppm	268	1170	366	163	Total LREE	ppm	9.11	6.66	10.01	0.9
Ni	ppm	34	25	68	181	Dy	ppm	2.8	2.4	4.1	0.4
Cr	ppm	70	25	5	15	Er	ppm	1.9	1.7	3.1	0.5
Cu	ppm	<1	173	3	11	Ho	ppm	0.6	0.6	0.9	0.1
P	ppm	290	100	300	90	Lu	ppm	0.26	0.27	0.44	0.07
S	ppm	<50	60	<50	320	Tb	ppm	0.36	0.34	0.53	0.05
Sc	ppm	42	44	17	3	Tm	ppm	0.3	0.2	0.5	<0.1
Ti	ppm	3280	2720	2300	210	Yb	ppm	2	1.7	3	0,4
V	ppm	194	279	47	300	Total HREE	ppm	8.22	7.21	12.57	1.52
Zn	ppm	13	79	31	11	Total REE	ppm	17.33	13.87	22.58	2.42
Ag	ppm	<0.1	<0.1	<0.1	<0.1	Al_2O_3	%	17.81	16.89	11.17	1.67
As	ppm	<1	1	<1	4	CaO	%	8.77	3.59	2.97	1.16
Ba	ppm	7	8	3	1	Cr_2O_3	%	0.03	0.01	<0.01	<0.01
Be	ppm	<0.5	<0.5	<0.5	<0.5	Fe_2O_3	%	5.42	11.71	6.12	87.7
Bi	ppm	<0.05	<0.05	<0.05	00.21	K_2O	%	0.15	0.14	0.02	<0.01
Cd	ppm	<0.05	<0.05	<0.05	<0.05	MgO	%	6.09	3.97	3.5	0.56
Co	ppm	27	85	18	82	MnO	%	0.04	0.18	0.06	0.02
Cs	ppm	0.3	0.1	<0.1	<0.1	Na_2O	%	3.84	3.21	1.56	0.04
Ga	ppm	15.4	13.6	11.8	10.6	P_2O_5	%	0.063	0.024	0.067	0.021
Ge	ppm	1.3	0.7	0.6	1.8	SiO_2	%	54.81	54.1	68.63	7.28
Hf	ppm	0.8	0.6	1.6	<0.1	TiO_2	%	0.58	0.44	0.41	0.04
In	ppm	<0.05	<0.05	<0.05	<0.05	S	%	<0.002	<0.002	<0.002	<0.002
Li	ppm	1.4	7	5.6	0.4	LOI	%	1.6	4.75	4.61	1.35
Mo	ppm	<0.1	<0.1	0.1	1.1	Total Major Oxide	%	99.26	99.01	99.121	99.85
Nb	ppm	0.2	0.2	0.4	<0.1						
Pb	ppm	<1	<1	<1	<1						
Rb	ppm	3.4	2.2	1.2	0.3						
Re	ppm	<0.05	<0.05	<0.05	<0.05						
Sb	ppm	<0.1	<0.1	<0.1	<0.1						
Se	ppm	<1	<1	<1	1						
Sn	ppm	0.6	0.2	1.6	0.4						
Sr	ppm	66.3	54.6	13.7	12.3						
Ta	ppm	<0.05	<0.05	<0.05	<0.05						
Te	ppm	<0.1	<0.1	<0.1	0.9						
Th	ppm	0.07	0.1	0.32	0.06						
Tl	ppm	0.02	0.03	<0.02	0.02						
U	ppm	<0.05	0.06	0.06	<0.05						
W	ppm	0.2	0.1	0.3	0.7						
Y	ppm	16.5	15.5	24.6	4.6						
Zr	ppm	15,1	12,3	25,9	1						
Total Tracer Element	ppm	4401.79	4879.45	3299.85	1428.39						

of the tholeiitic series is its high concentration of iron. Levels of alkaline elements, such as sodium and potassium, are comparatively lower (Du, 2023; Wang, 2022; Wang, 2022). Tholeiitic typically contains more silica (SiO_2) compared to other types of basalts, making it more similar to rhyolite in terms of magma evolution (Panda, 2023; Prostka, 1973). Volcanic Series Separation: This plot separates different types of volcanic series based on Co and Th content (Jafari, 2023; Járóka, 2023).

Rocks from the Tholeiitic Series tend to have higher Co values and lower Th values, which suggests they are more related to mantle magma and less affected by continental crust contamination (Ghoneim, 2023; Scoon, 2023; Thy, 2023). In contrast, rocks from the High-K Calc-Alkaline and Shoshonite Series have higher Th values and lower Co, indicating more significant differentiation and contamination processes (Yang, 2023; Zhang, 2023). Points in the Tholeiitic Series region suggest that the sample comes from basaltic rocks that form in mid-ocean ridge or hotspot environments (Carlson et al., 2018). The Tholeiite series is also shown in the Co-Th classification according to Hastie et al., in 2007. The TAS classification shows a theoliitic series (Fig. 8) (Raab and Spiro, 1991; Yoder, 1979).

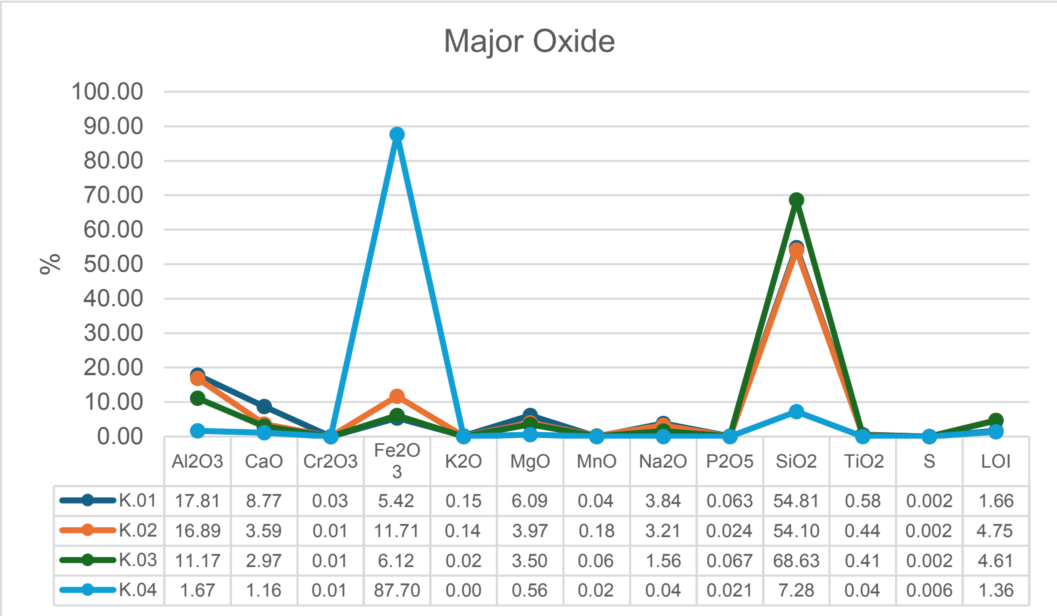

	Al2O3	CaO	Cr2O3	Fe2O3	K2O	MgO	MnO	Na2O	P2O5	SiO2	TiO2	S	LOI
K.01	17.81	8.77	0.03	5.42	0.15	6.09	0.04	3.84	0.063	54.81	0.58	0.002	1.66
K.02	16.89	3.59	0.01	11.71	0.14	3.97	0.18	3.21	0.024	54.10	0.44	0.002	4.75
K.03	11.17	2.97	0.01	6.12	0.02	3.50	0.06	1.56	0.067	68.63	0.41	0.002	4.61
K.04	1.67	1.16	0.01	87.70	0.00	0.56	0.02	0.04	0.021	7.28	0.04	0.006	1.36

Fig. 6. Comparison of Major Oxide K.01, K.02, K.03, and K.04

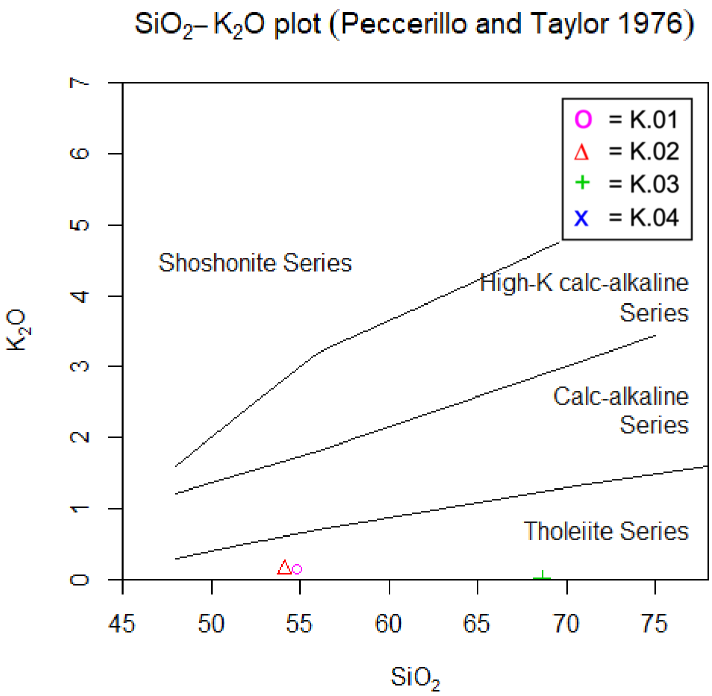

Fig. 7. Diagram of SiO2 - K2O Peccerilo and Taylor (1976) showing the tholeiite series

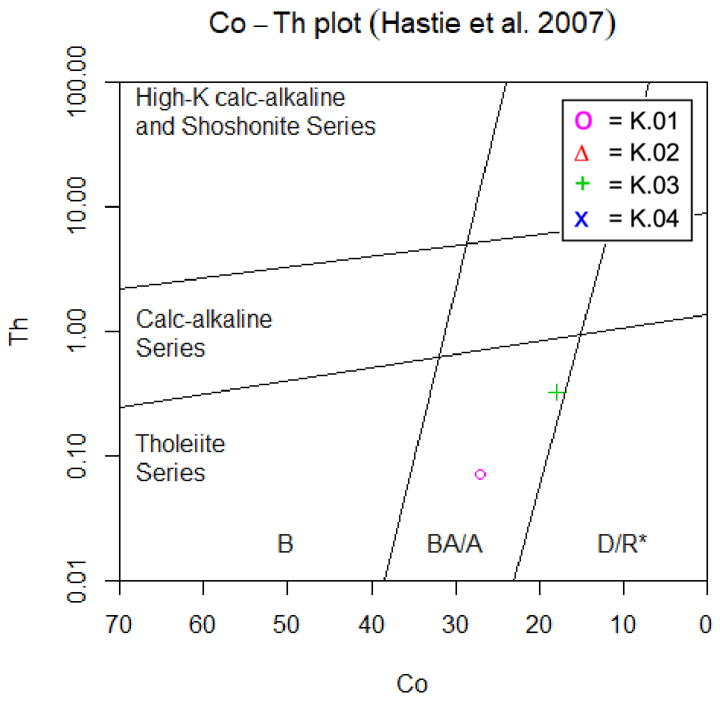

Fig. 8. Diagram of Co-Th plot (Hastie et al., 2007) shows tholeiite series

3.5. Tracer Element and Rare Earth Element Variations

Tracer and rare earth element analysis data can be used to identify rock or mineral sources and determine the environment of tectonic origin (He, 2022; Irzon, 2015). The highest tracer element composition is Ti and Mn (Fig. 9).

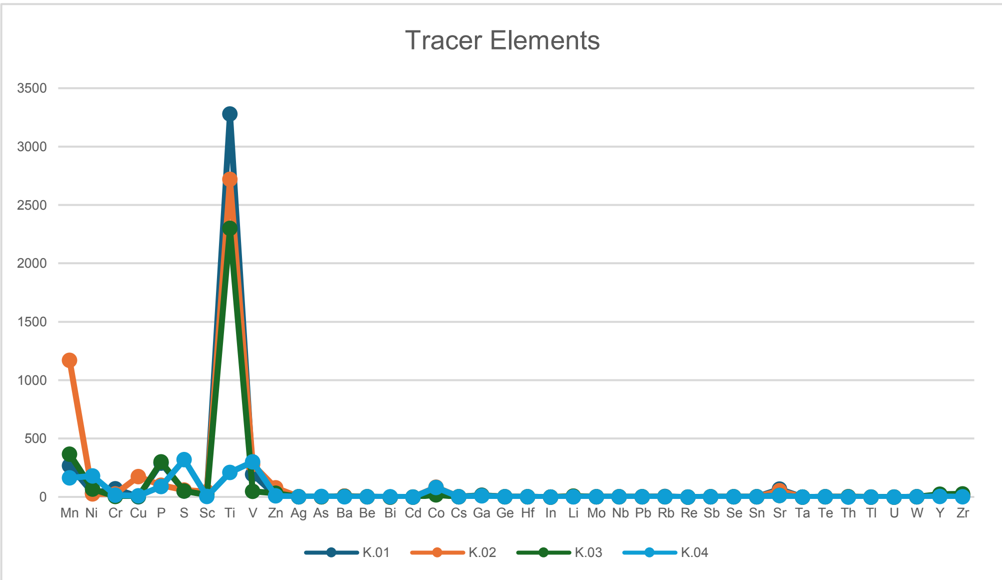

Fig. 9. Comparison chart of tracer elements

Spider plot is one of the visualization techniques used in petrology to show the distribution patterns of trace elements in a rock sample relative to a reference standard, such as a primitive mantle, chondrite, or crust composition (Wang, 2022; Zhou, 2022). Spider plot relative to the primitive mantle is used to indicate how much of a particular element in a rock has been enriched (positive anomalies) or thinned (negative anomalies) compared to a primitive mantle, which is considered to be the composition of the mantle that has not changed since the formation of the earth (Raimondo et al., 2017).

The Y-axis in this diagram uses a logarithmic scale to show the ratio between the concentration of elements in the sample and the reference value of the Primitive Mantle (Rahmani, 2020). A value of 1 on the Y axis indicates that the component is in the same concentration as the reference value of the Primitive Mantle (Datta, 2021). A value above 1 indicates enrichment, while a value below 1 indicates depletion relative to the primitive mantle (Shirmohammadi, 2023). The X-axis lists the various trace elements sorted by their geochemical properties. The horizontal line at Y = 1, this line serves as a reference to indicate the concentration of elements equivalent to the Primitive Mantle (Jiao et al., 2021). The data points located right on this line show elements with unchanged concentrations compared to the composition of the primitive mantle. Elements such as Cs, Ba, Rb, Th, and K show notable enrichment in most samples. These elements are mobile during subduction-related processes and are often enriched in volcanic arc settings due to the input of slab-derived fluids or melts into the mantle wedge. The enrichment of LILEs and depletion of HFSEs strongly indicate that a subduction zone setting influences the research area. The pattern of enrichment and thinning can be seen from the fluctuation of the line above and below the horizontal line at Y = 1 (Fig. 10) (Andrehs and Heinrich, 1998).

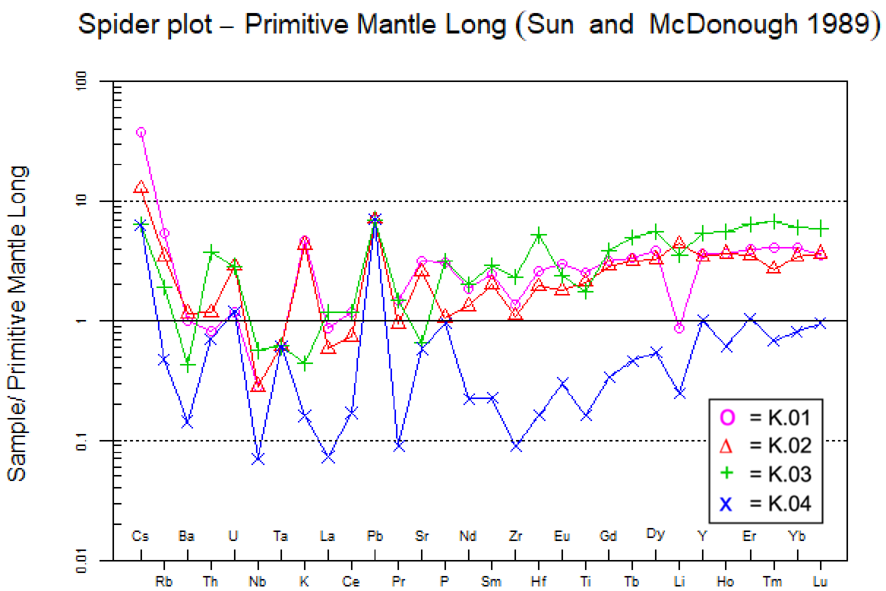

Fig. 10. Spider plot-primitive mantle long according to McDonough & Sun (1989) on tracer element

Some elements such as Ba, U, La, and Pb show significant enrichment, as their data points are well above the Y = 1 line. In contrast, elements such as Rb, Th, Nb, and some elements on the right (such as Er, Yb, Lu) show significant thinning because their points are well below the Y = 1 line (Rahmani, 2020). The elements Ba, U, La, and Pb undergo a very significant enrichment compared to the Primitive Mantle. This enrichment may be related to geological processes such as crystal fractionation or interactions with hydrothermal fluids that can enrich these elements in rocks(Datta, 2021; Shirmohammadi, 2023). Light Rare Earth Elements (LREE) such as La and Ce also undergo enrichment in these samples, which are often associated with magmatic differentiation (Walters et al., 2013). Depletion of the elements Rb, Th, and Nb indicates that these elements have been eliminated or not accumulated during the magmatism process that produced these rocks (Wang et al., 2023). Heavy Rare Earth Elements (HREE), such as Yb and Lu, also show thinning, which suggests that these rocks may have come from relatively small partial melts, where HREE is more concentrated in heavy minerals that do not melt (Andrehs and Heinrich, 1998; Jiao et al., 2021). Enrichment of certain elements, such as LREE and large lithophile elements (Ba, U, La, Pb), often indicates rocks formed from partial melts from mantle sources that undergo significant fractionation processes or the presence of contributions from the Earth's crust during magmatic processes (Zhao Id et al., 2024a; Zhao et al., 2023).

Depletion of certain elements, such as HREE, may indicate a condition of low partial melting or crystal fractionation in which heavy minerals such as garnet or amphibole hold the elements (Fig. 11) (Hopkins et al., 2021; McDonough and Sun, 1995).

Spider plot – this chondrite REE is used to understand the composition of REE elements in a sample relative to the primordial or reference composition (Anenburg, 2020). It provides insights into geological processes such as crystallization, fractionation, or metamorphism processes that affect the distribution of these elements within rocks or minerals. These graphs effectively visualize variations in REE composition in various samples, allowing for comparative analysis between samples and inference about possible geological processes. The X-axis displays the REE elements from the elements Lanthanum (La) to Lutetium (Lu). These REE elements are usually divided into Light REE (LREE) from La to Sm and Heavy REE (HREE) from Gd to Lu. These elements are ordered in order to facilitate the visualization of the distribution patterns of those elements (Zeng et al., 2024). The Y-axis uses a logarithmic scale that describes the ratio between the concentration of elements in a sample and the concentration of elements in chondrites (ancient meteorites often used as a reference for the composition of primordial elements). A line with a value of 1 on the Y axis (depicted with a dotted line) indicates that the concentration of the element in the sample is equivalent to the concentration in the chondrite. A value above 1 indicates that the element is more concentrated in the sample than the chondrite.

In contrast, a value below 1 indicates that the element is less concentrated in the sample than the chondrite (O'Neill, 2016). The green line (+), having a relatively stable distribution above reference line 1, indicates that this sample is rich in REE elements, particularly in heavy REEs (HREE) such as Dy, Ho, and Er. The red (triangle) and purple (round) lines show a lower distribution pattern of REE elements on certain elements than other lines but close to the reference line on heavy REEs. The blue line (x) has a distinct pattern, especially with significant increases in concentrations in heavy REEs such as Yb and Lu, but the concentration of these elements remains below 1 in most other elements, suggesting that this sample has a deficiency in terms of REE elements (Anenburg, 2020; O'Neill, 2016). Enrichment (increased concentration) in certain REE elements (e.g., HREE on the green line) suggests that geological processes affecting the sample may have led to accumulating these elements in higher amounts than chondrite. Depletion (decrease in concentration) on the blue line indicates that this sample is deficient in REE, possibly due to leaching or other geochemical processes that remove these elements (Fig. 11) (Zeng et al., 2024).

Ta/Yb is the ratio between Tantalum (Ta) and Ytterbium (Yb). Tantalum is a less common element and is usually associated with fractionation in magma, while Ytterbium is one of the Heavy Rare Earth Elements (HREE) (Shakerardakani et al., 2018). The X-axis operates on a logarithmic scale, with values from 0.01 to 100. The higher the value of Ta/Yb, the higher the ratio of Tantalum to Ytterbium in the rock, which often reflects more varied magmatism processes or in certain environments such as volcanic arcs (Zhao Id et al., 2024b). Th/Yb is the ratio between Thorium (Th) and Ytterbium (Yb). Thorium is an element usually associated with magma differentiation and sometimes with the mixing of crustal materials. Ytterbium, as mentioned earlier, is a heavy rare earth element. The Y-axis is also on a logarithmic scale, ranging from 0.01 to 100. The higher the Th/Yb value, the higher the Thorium content compared to Ytterbium, which often indicates a contribution from the continental crust or high fractionation (Fig. 12) (Irannezhadi et al., 2022; Wijaya and Setijadji, 2022).

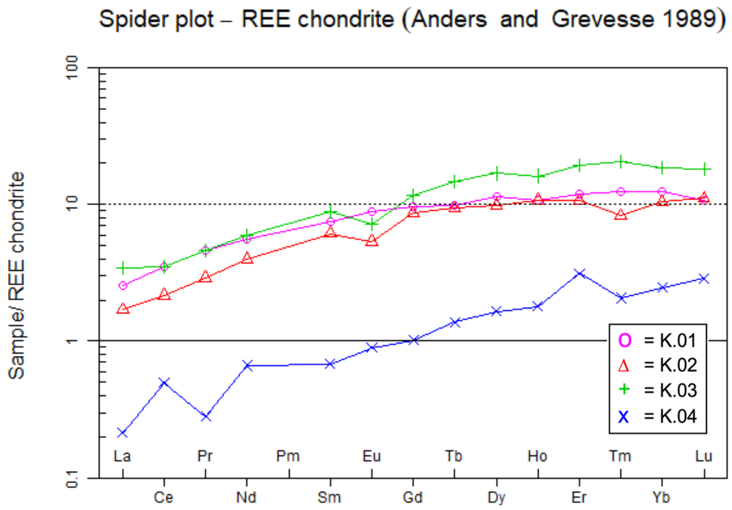

Fig. 11. Spider plot – REE Chondrite according to Anders and Grevesse Year, 1989

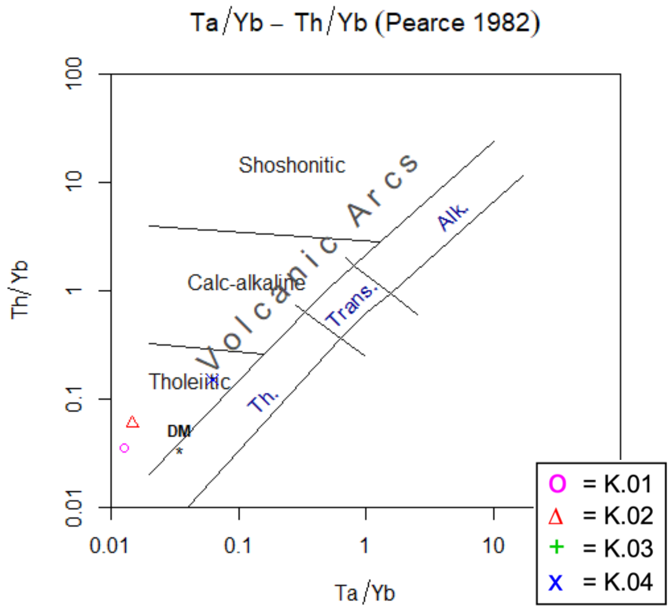

Fig. 12. Classification of Ta/Yb – Th/Yb according to Pearce (1982)

The graph shows that the tectonic environment is in the volcanic arcs with the tholeiitic magma series. Rocks in the Tholeiitic zone are generally formed in mid-ocean ridges or depleted mantle environments (Yan et al., 2019). These rocks typically have a low ratio of Th/Yb to Ta/Yb, which indicates the characteristics of basaltic magma originating from depleted mantle sources (Saccani et al., 2008). This distinguishes them from basaltic rocks that form in other environments, such as volcanic arc environments, which tend to have higher ratios due to the influence of subduction processes and crustal contamination (Saran, 2022).

4. Conclusions

The chemical composition of the research area shows that the rock types are andesite and basaltic andesite. The highest major oxide composition is the SiO2 compound, which is 54.81%; the second position is the Al2O3 compound, which is 17.81%. The highest major element composition is Fe, which is >50%, and the second is Al, which is 92,700 ppm. The highest tracer element composition is the Ti element, which is 3,280 ppm. Then the second is Mn 1,170 ppm. Several elements, such as Ba, U, and Pb, show significant enrichment. These data indicate that the research area is rich in REE elements, especially heavy REE (HREE) such as Dy, Ho, and Er. The nature of the rocks is included in the type of tholeiite series rocks in the research area. The tectonic environment is in a volcanic arc with a tholeiitic magma series.

References

Abbas, I.R.H., 2021. Petrology of ultramafic rocks from PT. Sebuku Iron Lateritic Ore (SILO) concession area and its effect on Ni and Fe in Sebuku Island, South Kalimantan, Indonesia. Institute of Physics Publishing Conference Series: Earth and Environmental Science, 921(1). doi.org/10.1088/1755-1315/921/1/012057.

Abbas, I.R.H., 2022. Petrology of ultramafic rocks from PT. Sebuku Iron Lateritic Ore (SILO) Concession Area, Sebuku Island, South Kalimantan, Indonesia. American Institute of Physics Conference Proceedings, 2543. https://doi.org/10.1063/5.0095501.

Aliyari, F., 2020. Geology, geochemistry, fluid inclusion and genesis of the Guijeh Qaleh IOA-type iron ore deposit, north of Takab district, Northwestern Iran. Ore Geology Reviews, 127. doi.org/10.1016/j.oregeorev.2020.103835.

Andrehs, G., Heinrich, W., 1998. Experimental determination of REE distributions between monazite and xenotime: potential for temperature-calibrated geochronology. Chemical Geology, 149(1–2), 83–96. doi.org/10.1016/s0009-2541(98)00039-4.

Anenburg, M., 2020. Rare earth mineral diversity controlled by REE pattern shapes. Mineralogical Magazine, 84(5), 629–639. https://doi.org/10.1180/MGM.2020.70.

Atapour, H., 2020. Comment on “Two-tiered magmatic-hydrothermal and skarn origin of magnetite from Gol-e-Ghohar iron ore deposit of SE Iran: In situ LA-ICP-MS analyses” by Mirzaei et al. (2018): (Ore Geology Reviews, 102, 639–653). Ore Geology Reviews, 127. https://doi.org/10.1016/j.oregeorev.2019.102942.

Bakri, H., 2023. Mineralogy and texture of the iron ore deposits in Tanjung and Pake, Bontocani, South Sulawesi, Indonesia. Institute of Physics Publishing Conference Series: Earth and Environmental Science, 1134(1). https://doi.org/10.1088/1755-1315/1134/1/012034.

Carlson, R.W., Grove, T.L., Donnelly-Nolan, J.M., 2018. Origin of primitive Tholeiitic and Calc-Alkaline Basalts at Newberry Volcano, Oregon. Geochemistry, Geophysics, Geosystems, 19(4), 1360–1377. https://doi.org/10.1029/2018GC007454

Chaerun, S., 2015. Isolation and phylogenetic characterization of iron-sulfur-oxidizing heterotrophic bacteria indigenous to nickel laterite ores of Sulawesi, Indonesia: Implications for biohydrometallurgy. American Institute of Physics, Conference Proceedings, 1677. https://doi.org/10.1063/1.4930772.

Chaerun, S.K., 2017. Bioleaching of supergene porphyry copper ores from Sungai Mak Gorontalo of Indonesia by an iron- and sulfur-oxidizing mixotrophic bacterium. Solid State Phenomena, 262, 20–23. https://doi.org/10.4028/www.scientific.net/SSP.262.20.

Coffield, D. Q., Bergman, Garrard, 1993. Tectonic and stratigraphic evolution of the Kalosi PSC area and associated development of a Tertiary petroleum system, South Sulawesi, Indonesia. In: Procceeding Indonesian Petrolium Association, 22nd. Available at: https://www.ipa.or.id/en/publications/tectonic-and-stratigraphic-evolution-of-the-kalosi-psc-area-and-associated-development-of-a-tertiary-petroleum-system-south-sulawesi-indonesia.

Cox, K.G., Bell, J.D., Pankhurst, R.J., 1979. The Interpretation of Igneous Rocks. https://doi.org/10.1007/978-94-017-3373-1.

Datta, P., 2021. Origin of Ni-Cu-(PGE + Au) sulfides in Late-Archean komatiitic suite of rocks in the Shankaraghatta belt, Western Dharwar Craton (India). Ore Geology Reviews, 138. https://doi.org/10.1016/j.oregeorev.2021.104375.

Djuri, Sudjatmiko, Bachri, S., Sukido, 1998. Peta Geologi Lembar Majene dan Bagian Barat Lembar Palopo, Sulawesi. Bandung.

Dong, R., 2021. The geology, magnetite geochemistry, and oxygen isotopic composition of the Akesayi skarn iron deposit, Western Kunlun Orogenic Belt, Xinjiang, northwest China: Implications for ore genesis. Ore Geology Reviews, 130. https://doi.org/10.1016/j.oregeorev.2020.103854.

Du, Q., 2023. New ages of Early Cretaceous magmatic rocks in the Yanbian area (NE China): implications for the subduction and slab rollback of the Paleo-Pacific Plate beneath eastern China during Early Cretaceous. International Geology Review, 65(1), 154–178. https://doi.org/10.1080/00206814.2022.2037109.

Duan, S., 2014. Geology, geochemistry, and geochronology of the Dunde iron-zinc ore deposit in Western Tianshan, China. Ore Geology Reviews, 57, 441–461. https://doi.org/10.1016/j.oregeorev.2013.08.019.

Dwivedy, S., 2021. Geology and trace element geochemistry of the albite hosted iron ore mineralization around Khetri copper deposit, India: Implications for an IOA type deposit. Ore Geology Reviews, 138. https://doi.org/10.1016/j.oregeorev.2021.104343.

Gao, Q.J., 2017. Influence and mechanism of Indonesia vanadium titano-magnetite on metallurgical properties of iron ore sinter. Journal of Central South University, 24(12), 2805–2812. https://doi.org/10.1007/s11771-017-3695-2.

Gerlitzki, M., 2023. Geology and geochemistry of iron ores from the Black Forest and its foreland under specific consideration of their content of rare earth elements (REE). Zeitschrift der Deutschen Gesellschaft fur Geowissenschaften, 174(4), 675–711. https://doi.org/10.1127/zdgg/2023/0392.

Gest , D.E., McBirney, A.R., 1979. Genetic relations of shoshonitic and absarokitic magmas, Absaroka Mountains, Wyoming. Journal of Volcanology and Geothermal Research, 6(1–2), 85–104. https://doi.org/10.1016/0377-0273(79)90048-9.

Ghoneim, M.M., 2023. Analytical methodology for geochemical features and radioactive elements for intrusive rocks in El Sela area, Eastern Desert, Egypt. International Journal of Environmental Analytical Chemistry, 103(6), 1272–1291. https://doi.org/10.1080/03067319.2021.1873310.

Godang, S., Priadi, B., Fadlin, Van Leeuwen, T., Idrus, A., 2021. Geochemistry study of cross-clastic magma alkalinity evolution. Indonesian Journal on Geoscience, 8(2), 177–196. https://doi.org/10.17014/IJOG.8.2.177-196.

Hakim, M.M. Al, Idrus, A., Suryanto, W., Raharjanti, N.A., Ananke, P.D., Ernowo, E., Pardiarto, B., 2024. Ore characteristics and distribution based on geological and geophysical features of the Tambang Sawah low sulfidation epithermal gold prospect in Lebong District, Sumatra Island, Indonesia. Iraqi Geological Journal, 57(2B), 219–239. https://doi.org/10.46717/IGJ.57.2B.15MS-2024-8-25.

Hall, R., 2013. The paleogeography of Sundaland and Wallacea since the Late Jurassic. Journal of Limnology, 72(S2), 1–17. https://doi.org/10.4081/JLIMNOL.2013.S2.E1.

Han, S.L., 2012. REE geochemistry application in discrimination of metallogenic system and ore genesis: An example from iron polymetallic orefield in Taliabu Island, Indonesia. Zhongguo Youse Jinshu Xuebao/Chinese Journal of Nonferrous Metals, 22(3), 784–794. Available at: https://www.scopus.com/inward/record.uri?partnerID=HzOxMe3b&scp=84862313392&origin=inward

Hanžl, P., Janoušek, V., Hrdličková, K., Buriánek, D., Gerel, O., Altanbaatar, B., Hora, J.M., Čoupek, P., 2023. From magmatic arc to a post-accretionary setting: Late Palaeozoic granitoid plutons in the northwestern Trans-Altai Zone, Mongolia. Journal of Geosciences, 68(1), 25–66. https://doi.org/10.3190/JGEOSCI.366.

He, S., 2022. Petrogenesis and tectonic implications of the late Neoproterozoic mafic dykes in the South Qinling Belt, China. Precambrian Research, 373. https://doi.org/10.1016/j.precamres.2022.106647.

Hopkins, J.L., Bidmead, J.E., Lowe, D.J., Wysoczanski, R.J., Pillans, B.J., Ashworth, L., Rees, A.B.H., Tuckett, F., 2021. TephraNZ: a major- And trace-element reference dataset for glass-shard analyses from prominent Quaternary rhyolitic tephras in New Zealand and implications for correlation. Geochronology, 3(2), 465–504. https://doi.org/10.5194/GCHRON-3-465-2021.

Hou, T., 2014. Geology, tectonic settings and iron ore metallogenesis associated with submarine volcanism in China: An overview. Ore Geology Reviews, 57, 498–517. https://doi.org/10.1016/j.oregeorev.2013.08.007.

Irannezhadi, M.R., Ghorbani, M.R., Hoernle, K.A., Tavakoli, N., Namnabat, E., Hauff, F., Hansteen, T., 2022. Geochemistry and petrogenesis of tertiary subvolcanics from north Tehran, southern Central Alborz (Iran). Arabian Journal of Geosciences, 15(4), 1–24. https://doi.org/10.1007/S12517-022-09604-3.

Irzon, R., 2015. Contrasting two facies of muncung granite in Lingga Regency using major, trace, and rare earth element geochemistry. Indonesian Journal on Geoscience, 2(1), 23–33. https://doi.org/10.17014/IJOG.2.1.23-33.

Jafari, A., 2023. Geologic history of the Sabzevar oceanic Basin, NE Iran: An overview from continental rifting to obduction in the NeoTethys oceanic system. Journal of Asian Earth Sciences, 245. https://doi.org/10.1016/j.jseaes.2023.105559.

Járóka, T., 2023. Age and petrogenesis of Ni-Cu-(PGE) sulfide-bearing gabbroic intrusions in the Lausitz Block, northern Bohemian Massif (Germany/Czech Republic). Lithos, 444. https://doi.org/10.1016/j.lithos.2023.107090.

Jensen, L.S., 1976. A New Cation Plot For Classifying Subalkalic Volcanic Rocks. Ministry of Natural Resources.

Jiao, S., Evans, N.J., Mitchell, R.N., Fitzsimons, I.C.W., Guo, J., 2021. Heavy rare-earth element and Y partitioning between monazite and garnet in aluminous granulites. Contributions to Mineralogy and Petrology, 176(7), 1–20. https://doi.org/10.1007/S00410-021-01808-2/METRICS.

Karimi, P., 2021. Geology and geochemistry of bukan iron ore deposits, ductile shear zone, Northwest Iran. Neues Jahrbuch fur Mineralogie, Abhandlungen, 197(2), 121–144. https://doi.org/10.1127/njma/2021/0262.

Keshava, K., Kumar, P.L., 2020. Geochemical characteristics of iron ore deposits and processing of Landsat-8 data (geology, geomorphology and lineaments) in semi-arid region and using geospatial techniques. Modeling Earth Systems and Environment, 6(2),1245–1252. https://doi.org/10.1007/s40808-020-00754-5.

Kusnadi, F., 2018. Reduction of Indonesia iron ore using biomass palm kernel shell charcoal: Effect of residence time. AIP Conference Proceedings, 1977. https://doi.org/10.1063/1.5042891.

Li, G., 2014. Comment on 'Geochronology and geochemistry of submarine volcanic rocks in the Yamansu iron deposit, Eastern Tianshan Mountains, NW China: Constraints on the metallogenesis' by Tong Hou, Zhaochong Zhang, M. Santosh, John Encarnacion, Jiang Zhu, Wenjuan Luo. Ore Geology Reviews, 63, 343–345. https://doi.org/10.1016/j.oregeorev.2014.04.014.

McDonough, W.F., Sun, S.S., 1989. The composition of the Earth. Chemical Geology, 120(3–4), 223–253. https://doi.org/10.1016/0009-2541(94)00140-4.

O'Neill, H.S.C., 2016. The smoothness and shapes of chondrite-normalized rare earth element patterns in basalts. Journal of Petrology, 57(8), 1463–1508. https://doi.org/10.1093/PETROLOGY/EGW047.

Osterholt, V., 2018. Simulation of orebody geology with multiple-point geostatistics-application at Yandi channel iron ore deposit, WA, and implications for resource uncertainty. Advances in Applied Strategic Mine Planning, 335–352. https://doi.org/10.1007/978-3-319-69320-0_22.

Panda, A., 2023. Precise Pb-Pb baddeleyite geochronology, geochemistry, and Sr-Nd isotopic constraints on the 2.36 & 1.88 Ga mafic dykes from the Bastar craton, India: Implications for their petrogenesis in conjunction with the Dharwar mafic dykes. Precambrian Research, 393. https://doi.org/10.1016/j.precamres.2023.107090.

Pearce, J.A., 1982. Trace Element Characteristics of Lavas from Destructive Plate Boundaries. In: Thorpe, R.S., (Ed.), Andesites. Wiley, Chichester, 525–548.

Peccerillo, A., Taylor, S.R., 1976. Geochemistry of Eocene calc-alkaline volcanic rocks from the Kastamonu area, Northern Turkey. Contributions to Mineralogy and Petrology, 58(1), 63–81. https://doi.org/10.1007/BF00384745/METRICS.

Philpotts, A.R., Ague, J.J., 2022. Principles of Igneous and Metamorphic Petrology. https://doi.org/10.1017/9781108631419.

Poojari, M., Vardhan, H., Jathanna, H.M., 2023. Iron ore characterization techniques in mineral processing. Journal of The Institution of Engineers (India), 105(1), 543–551. https://doi.org/10.1007/S40033-023-00483-W.

Prostka, H.J., 1973. Hybrid origin of the absarokite-shoshonite-banakite series, Absaroka Volcanic Field, Wyoming. GSA Bulletin, 84(2), 697–702. https://doi.org/10.1130/0016-7606(1973)84<697:HOOTAS>2.0.CO;2.

Raab, M., Spiro, B., 1991. Sulfur isotopic variations during seawater evaporation with fractional crystallization. Chemical Geology: Isotope Geoscience section, 86(4), 323–333. https://doi.org/10.1016/0168-9622(91)90014-N.

Rahmani, F., 2020. Petrology and geochemistry of mafic and ultramafic cumulate rocks from the eastern part of the Sabzevar ophiolite (NE Iran): Implications for their petrogenesis and tectonic setting. Geoscience Frontiers, 11(6), 2347–2364. https://doi.org/10.1016/j.gsf.2020.02.004.

Raimondo, T., Payne, J., Wade, B., Lanari, P., Clark, C., Hand, M., 2017. Trace element mapping by LA-ICP-MS: assessing geochemical mobility in garnet. Contributions to Mineralogy and Petrology, 172(4), 1–22. https://doi.org/10.1007/S00410-017-1339-Z.

Rochani, S., Sariman, S., Anugrah, R.I., Pramusanto, P., 2008. The current status of iron minerals in Indonesia. Indonesian Mining Journal, 11(2), 1–17.

Saccani, E., Principi, G., Garfagnoli, F., Menna, F., 2008. Corsica ophiolites: geochemistry and petrogenesis of basaltic and metabasaltic rocks. Ofioliti, 33(2), 187–207.

Saran, R., 2022. Trace Element Analysis: Methodology, Instrumentation, Analytical Performance and Application. Analytical Techniques for Trace Elements in Geochemical Exploration, 1–28. https://doi.org/10.1039/9781839166518-00001.

Scoon, R.N., 2023. Petrogenesis of the Marginal Sill Phase and Lower Zone in the Eastern Limb of the Bushveld Complex: Incremental development of igneous layering and syn-magmatic emplacement of peridotite intrusions and sills. South African Journal of Geology, 126(4), 425–450. https://doi.org/10.25131/sajg.126.0021.

Shah, A.K., Taylor, R.D., Walsh, G.J. and Phillips, J.D., 2021. Integrated geophysical imaging of rare-earth-element-bearing iron oxide-apatite deposits in the eastern Adirondack Highlands, New York. Geophysics, 86(1), B37–B54. https://doi.org/10.1190/GEO2019-0783.1.

Shakerardakani, F., Neubauer, F., Liu, X., Bernroider, M., Monfaredi, B. and von Quadt, A., 2018. Tectonic significance of Triassic mafic rocks in the June Complex, Sanandaj–Sirjan zone, Iran. Swiss Journal of Geosciences, 111(1–2), 13–33. https://doi.org/10.1007/S00015-017-0281-4/FIGURES/13.

Shirmohammadi, M., 2023. Geochemistry and Sr-Nd isotopic characteristics of ferroan-magnesian metaluminous granites of the NW Sanandaj-Sirjan zone, Iran: Granite formation in a compressional-extensional setting during Late Jurassic time. Geological Magazine, 160(6), 1065–1089. https://doi.org/10.1017/S0016756823000146.

Soedarsono, J.W., 2013. Potential indonesia ores as raw material for producing iron nugget. Advanced Materials Research, 652, 2529–2533. https://doi.org/10.4028/www.scientific.net/AMR.652-654.2529.

Spier, C.A., de Oliveira, S.M.B., Rosière, C.A., Ardisson, J.D., 2007. Mineralogy and trace-element geochemistry of the high-grade iron ores of the Águas Claras Mine and comparison with the Capão Xavier and Tamanduá iron ore deposits, Quadrilátero Ferrífero, Brazil. Mineralium Deposita, 43(2), 229–254. https://doi.org/10.1007/S00126-007-0157-Z.

Tamehe, L.S., 2019. Geology of the Gouap iron deposit, Congo craton, southern Cameroon: Implications for iron ore exploration. Ore Geology Reviews, 107, 1097–1128. https://doi.org/10.1016/j.oregeorev.2019.03.034.

Thamsi, A.B., Bakri, H., Harwan, H., Nasrullah, N., Aswadi, M., 2021. Karakteristik Mineralogi Bijih Besi Daerah Kadong-Kadong, Kabupaten Luwu, Provinsi Sulawesi Selatan. Jurnal Pertambangan, 5(4), 158–164. https://doi.org/10.36706/jp.v5i3.454.

Thy, P., 2023. Petrology of the Skaergaard layered series. GEUS Bulletin, 56. https://doi.org/10.34194/geusb.v56.8327.

Vermeesch, P., Pease, V., 2021. A genetic classification of the tholeiitic and calc-alkaline magma series. Geochemical Perspectives Letters, 19, 1–6. https://doi.org/10.7185/GEOCHEMLET.2125

Wakila, M.H., Nompo, S., Jafar, N., Thamsi, A.B., Munir, A.S., Heriansyah, A.F., 2024. Analysis of cobalt distribution and Co-Ni correlation in nickel laterite zonation in tropical region. Iraqi Geological Journal, 57(2B), 205–218. https://doi.org/10.46717/IGJ.57.2B.14MS-2024-8-24.

Walters, A.S., Goodenough, K.M., Hughes, H.S.R., Roberts, N.M.W., Gunn, A.G., Rushton, J., Lacinska, A., 2013. Enrichment of rare earth elements during magmatic and post-magmatic processes: A case study from the Loch Loyal Syenite Complex, northern Scotland. Contributions to Mineralogy and Petrology, 166(4), 1177–1202. https://doi.org/10.1007/S00410-013-0916-Z/FIGURES/12.

Wang, C.L., 2022a. Genesis of the Kiruna-type Nixintage iron deposit, Chinese Western Tianshan, NW China: Constrains of ore geology, geochemistry and geochronology. Journal of Geochemical Exploration, 243. https://doi.org/10.1016/j.gexplo.2022.107094.

Wang, C.L., 2024. Ore Geology, H-O-C Isotopes and 40Ar-39Ar Dating of the Wutonggou Iron Deposit, Eastern Tianshan, NW China: Implications for the source, timing, and genesis of hydrothermal mineralization in a sedimentary iron deposit. Journal of Earth Science, 35(4), 1170–1185. https://doi.org/10.1007/s12583-022-1686-1.

Wang, J., 2022b. Geochronology and geochemistry of 2.3 Ga mafic intrusions in the Dengfeng area: Evidence for early Paleoproterozoic subduction in the southern North China Craton. Precambrian Research, 375. https://doi.org/10.1016/j.precamres.2022.106668.

Wang, X., 2022c. Geochemical constraints on the nature of Late Archean basaltic-andesitic magmatism in the North China Craton. Earth-Science Reviews, 230. https://doi.org/10.1016/j.earscirev.2022.104065.

Wang, Y., 2022d. Early Cretaceous subduction in NW Kalimantan: Geochronological and geochemical constraints from the Raya and Mensibau igneous rocks. Gondwana Research, 101, 243–256. https://doi.org/10.1016/j.gr.2021.08.006.

Wang, Y., Liu, L., Sun, M., Huang, J., Huang, Y., Liang, X., Tan, W., He, H. and Zhu, J., 2023. Distribution and fractionation of rare earth elements (REE) in the Ion Adsorption-type REE Deposit (IAD) at Maofeng Mountain, Guangzhou, China. Clays and Clay Minerals, 71(3), 340–361. https://doi.org/10.1007/S42860-023-00251-7/METRICS.

White, L.T., Hall, R., Armstrong, R.A., Barber, A.J., BouDagher Fadel, M., Baxter, A., Wakita, K., Manning, C. and Soesilo, J., 2017. The geological history of the Latimojong region of western Sulawesi, Indonesia. Journal of Asian Earth Sciences, 138, 72–91. https://doi.org/10.1016/J.JSEAES.2017.02.005.

Wijaya, M.E.J. and Setijadji, L.D., 2022. A preliminary volcanological study of north eastern Kaba Volcano, Bengkulu Province, Indonesia. Institute of Physics Publishing Conference Series: Earth and Environmental Science, 1071(1). https://doi.org/10.1088/1755-1315/1071/1/012018.

Winter, J.D., 2014. Principles of Igneous and Metamorphic Petrology (2nd ed.) London: Pearson. Available.

Yan, Q., Zhang, P., Metcalfe, I., Liu, Y., Wu, S., Shi, X., 2019. Geochemistry of axial lavas from the mid-and southern Mariana Trough, and implications for back-arc magmatic processes. Mineralogy and Petrology, 113(6), 803–820. https://doi.org/10.1007/S00710-019-00683-X/METRICS.

Yang, C.X., 2023. The Coorg Block, southern India: Insights from felsic and mafic magmatic suites on Mesoarchean plate tectonics and correlation with supercontinent Ur. Gondwana Research, 118, 1–36. https://doi.org/10.1016/j.gr.2023.02.015.

Yoder, H.S., 1979. Evolution of the Igneous Rocks. Princeton University Pres.

Zarasvandi, A., Rezaei, M., Sadeghi, M., Pourkaseb, H., Sepahvand, M., 2016. Rare-earth element distribution and genesis of manganese ores associated with Tethyan ophiolites, Iran: A review. Mineralogical Magazine, 80(1), 127–142. https://doi.org/10.1180/MINMAG.2016.080.054.

Zeng, L., Peng, T., Sun, H., Zhang, X., Zhao, D., 2024. Comparative study on ionic dissolution and structural changes of montmorillonite, kaolinite, and muscovite during interfacial reactions with oxalic acid solution. Mineralogical Magazine, 1–29. https://doi.org/10.1180/MGM.2024.31.

Zhang, L., 2023. Geochemical and thermodynamic constraints on Archean comagmatic volcanic and cumulate rocks from southern West Greenland. Geochimica et Cosmochimica Acta, 348, 122–139. https://doi.org/10.1016/j.gca.2023.03.005.

Zhao Id, Z., Li, Z., Li, H., Cheng, B., Yin, Y., 2024a. Geochronology, geochemistry, and geological significance of early Jurassic intrusive rocks in the Lesser Xing'an- Zhangguangcai Range, northeast China. PLOS ONE, 19(8), e0306465. https://doi.org/10.1371/JOURNAL.PONE.0306465.

Zhao Id, Z., Li, Z., Li, H., Cheng, B., Yin, Y., 2024b. Geochronology, geochemistry, and geological significance of early Jurassic intrusive rocks in the Lesser Xing'an- Zhangguangcai Range, northeast China. PLOS ONE, 19(8), e0306465. https://doi.org/10.1371/JOURNAL.PONE.0306465.

Zhao, Y., Huang, F., Wang, D., Wei, N., Zhao, C., Liu, Z., 2023. U-Pb geochronology, geochemistry and geological significance of the Yongfeng composite granitic pluton in southern Jiangxi Province. Minerals, 13(11), 1457. https://doi.org/10.3390/MIN13111457/S1.

Zhou, X., 2022. The latest Neoproterozoic basaltic and siliciclastic rocks and tectonic implications in the Tarim Craton, NW China. Journal of Asian Earth Sciences, 232. https://doi.org/10.1016/j.jseaes.2022.105148.